ANALYSIS OF CONCRETE FRACTURE IN "DIRECT" TENSION

Jan G. Rots and René de Borst

Delft University of Technology, Department of Civil Engineering/TNO Institute for Building
Materials and Structures, P.O. Box 5048, 2600 GA Delft, The Netherlands

Abstract—The direct tension test on concrete specimens is analysed using finite elements. The analysis shows that the behaviour after peak load is strongly non-homogeneous and involves asymmetric crack propagation. These observations, which are supported by experimental evidence, have consequences for deriving "stress–strain" relations from direct tension tests, since they demonstrate that the observed softening behaviour is partially a structural effect. Attention is furthermore drawn to the possibility of snap-back behaviour in strain-softening concrete and to consequences thereof for numerical and experimental investigations.

1. INTRODUCTION

One of the most interesting phenomena in concrete and rock-like materials in tension is the fact that the load–displacement curve displays a gradual descending branch after attaining the peak load. Upon translation of such a load–displacement curve into a stress–strain curve, two problems arise. First, the stress–strain curve, which is usually obtained by dividing the load by the original load carrying cross-section and the displacement by the original length, can neither be classified as elastic-perfectly brittle, nor as elastic-perfectly plastic. Instead, we must utilize an elastic-softening formulation, which has first been recognized by Hillerborg *et al.* (1976) and Bažant and Oh (1983).

The other problem is that strain-softening is nearly always accompanied by non-homogeneous and highly localized deformations of the specimen (Cornelissen *et al.*, 1986; Hordijk *et al.*, 1987; Labuz *et al.*, 1985; van Mier, 1986; Read and Hegemier, 1984). The issue is whether the observed drop in the load–displacement curve is really a material property or whether it is a structural effect that is purely a consequence of the experimentally observed non-homogeneous deformations. In the past, several contributions in the literature have been devoted to this debate, but many discussions pertain to compressive loadings (van Mier, 1986; Read and Hegemier, 1984). In this paper we will concentrate on tensile loading.

We will show that non-homogeneous deformations in the post-failure regime may strongly affect the resulting load–displacement curve, for the same set of material parameters may result in a completely different load–displacement curve, depending on the failure mechanism that is triggered. Yet, this observation should not tempt one to conclude that softening type constitutive formulations must be abandoned. Instead, such analyses may assist in developing stress–strain relations at a local level which can reproduce the observed phenomena at a structural level.

Another issue to which attention will be drawn is snap-back behaviour which may occur in strain softening materials under quasi-static loading conditions (de Borst, 1986; Carpinteri *et al.*, 1986; Crisfield, 1986). In the present paper we will show that this phenomenon also dominates the response of concrete in a direct tensile test. This observation imposes severe demands on testing procedures as well as on computational strategies.

After reviewing the experimental progress in uniaxial testing of plain concrete and rock and discussing the relevant numerical techniques, we will analyse the direct tensile test on concrete with the aid of finite elements. Here, the problem is posed in two different ways. On one hand, an analysis has been carried out for a specimen that does not contain imperfections, so that we have a bifurcation problem, while in the other analyses an imperfection has been inserted in the finite element model. Furthermore, the role of the
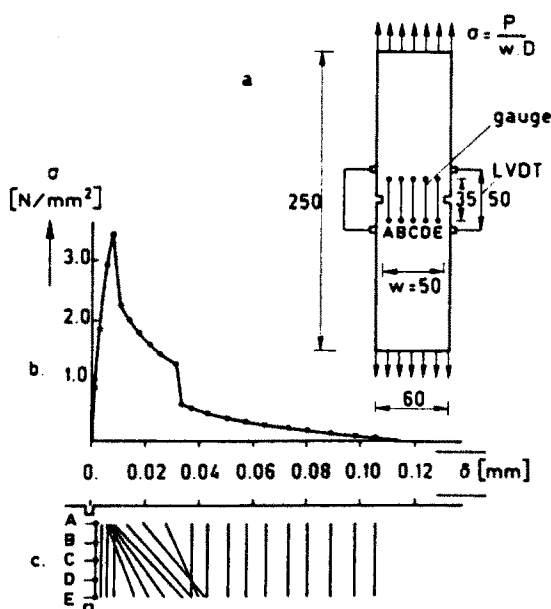
Fig. 1. Experimental results for the direct tensile test (Cornelissen *et al.*, 1986 ; Hordijk *et al.*, 1987).
(a) Specimen and instrumentation. (b) Average stress-deformation curve over a 35 mm gauge length.
(c) Distribution of deformation over the cross-section between the notches.

boundary conditions in triggering localization and non-homogeneous deformations is analysed.

2. EXPERIMENTAL ASPECTS

Direct tensile tests have been carried out at the Stevin Laboratory of Delft University of Technology by Cornelissen *et al.* (1986) and Hordijk *et al.* (1987). The specimens were double-notched prisms 250 mm long, 60 mm wide and 50 mm thick (Fig. 1a) and were tested in a closed loop electro-hydraulic testing machine. The maximum size of the light-weight aggregate was 8 mm.

A typical result is shown in Fig. 1b, which gives an average stress-deformation curve. Here, the average stress is defined as the load divided by the original net cross-sectional area (50×50 mm^2), while the deformation is the averaged result of ten extenso-meters, five at the front and five at the back of the specimen, as indicated by A to E in Fig. 1a. The gauge length of the extenso-meters was 35 mm, which will serve as a reference length throughout this paper unless specified otherwise. The diagram of Fig. 1b shows that the stress increases almost linearly up to the peak stress, whereafter a steep drop occurs which gradually evolves into a long tail. Although the load and the displacements in the softening part of the load–displacement curve could be controlled completely and could be registered properly, there remains the curious observation of a pronounced "bump" half-way down the softening branch. Similar "bumps" in softening curves from direct tensile tests have been reported amongst others by Willam *et al.* (1986) and Budnik (1985).

Another view of the experimental results is presented in Fig. 1c, where the separate readings of the extenso-meters A to E have been plotted for various stages of the deformation process. Prior to the peak stress the deformation distribution over the centre section appears to be symmetric, but immediately after passing the peak stress we observe non-symmetric deformations which reveal that the fracture tends to propagate from one side of the specimen to the other rather than propagating symmetrically. Non-symmetric tensile fracture modes have also been reported by Labuz *et al.* (1985), although others claim to have observed symmetric modes, e.g. Gopalaratnam and Shah (1985).

The observation of a non-symmetric fracture mode is of utmost importance as it in fact suggests that the "direct" tensile test is not as direct as has been assumed so far. Indeed, the issue has also been recognized by Hordijk *et al.* (1987), who advocated the idea

that there might be an interrelation between the "bump" and the non-homogeneous deformations. A sound explanation of these phenomena can be provided with aid of numerical simulations.

3. CONSTITUTIVE ASPECTS

The constitutive model that has been employed in the analyses is formulated within the smeared crack concept and has been developed by de Borst and Nauta (1985) and Rots *et al.* (1985). The model is based upon a decomposition of the total strain rate into a concrete strain rate $\dot{\varepsilon}^{co}$ and a crack strain rate $\dot{\varepsilon}^{cr}$:

$$\dot{\varepsilon} = \dot{\varepsilon}^{co} + \dot{\varepsilon}^{cr}. \tag{1}$$

This decomposition allows for separate formulations of the stress–strain law for the crack and the constitutive model for the intact concrete between the cracks. In the present paper we will confine ourselves to linear-elastic behaviour of the concrete and to a softening model for the cracks, so that we arrive at an elastic-softening model for the cracked concrete.

The relation between the crack strain rate of a particular crack and the stress rate is conveniently defined in the coordinate system which is aligned with the crack. This necessitates a transformation between the crack strain rate $\dot{\varepsilon}^{cr}$ in the global x, y, z coordinates and a crack strain rate $\dot{e}^{cr}$ which is expressed in local coordinates. For a two-dimensional configuration, we observe that a crack only has a normal strain rate $\dot{e}^{cr}_{nn}$ (mode-I, crack opening) and a shear strain rate $\dot{e}^{cr}_{nt}$ (mode-II, crack sliding), so that $\dot{e}^{cr} = (\dot{e}^{cr}_{nn} \, \dot{e}^{cr}_{nt})^{T}$ where the superscript T denotes a transpose. The relation between $\dot{\varepsilon}^{cr}$ and $\dot{e}^{cr}$ reads

$$\dot{\varepsilon}^{cr} = N\dot{e}^{cr} \tag{2}$$

with N a $3 \ast 2$ transformation matrix (de Borst and Nauta, 1985; Rots *et al.*, 1985). We can furthermore define a vector $\dot{s} = (\dot{s}_{nn}\dot{s}_{nt})^{T}$ with $\dot{s}_{nn}$ the normal and $\dot{s}_{nt}$ the shear stress rate in the crack. The relation between the stress rate in the global coordinate system $\dot{\sigma}$ and the stress vector $\dot{s}$ reads in a similar fashion

$$\dot{s} = N^{T}\dot{\sigma}. \tag{3}$$

To complete the system of equations, we need a constitutive model for the intact concrete and a stress–strain relation for the smeared cracks. When D^{e} denotes the elasticity matrix, we have for the present case of linear-elastic behaviour of the concrete between the cracks

$$\dot{\sigma} = D^{e}\dot{\varepsilon}^{co}. \tag{4}$$

In a similar fashion, we can postulate a relation between the crack strain rate $\dot{e}^{cr}$ and the stress rate $\dot{s}$ in the crack. In this paper a relation has been assumed which formally reads :

$$\dot{s} = D^{cr}\dot{e}^{cr} \tag{5}$$

with D^{cr} a $2 \ast 2$ matrix that incorporates the constitutive properties of the (smeared-out) cracks. Combination of eqns (1)–(5) then results in the stress–strain relation for the cracked concrete :

$$\dot{\sigma} = \{D^{e} - D^{e}N[D^{cr} + N^{T}D^{e}N]^{-1}N^{T}D^{e}\}\dot{\varepsilon}. \tag{6}$$

In the present study coupling terms, which for instance occur in crack-dilatancy theories, e.g. Walraven and Reinhardt (1981), between the shear stress rate $\dot{s}_{nt}$ and the normal crack strain rate $\dot{e}^{cr}_{nn}$, or between the normal stress rate $\dot{s}_{nn}$ and the shear crack strain rate $\dot{e}^{cr}_{nt}$ are not relevant. Consequently, these terms have been set equal to zero in D^{cr}. Furthermore,
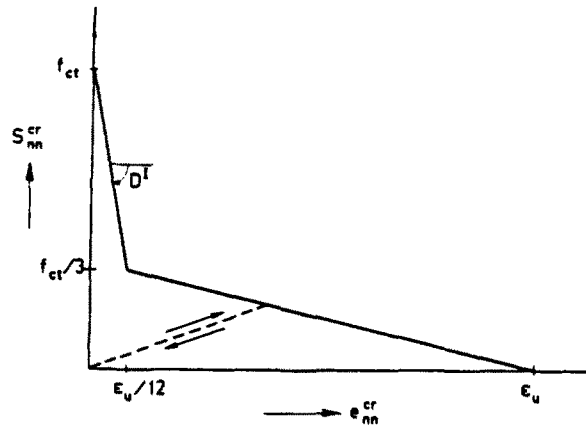
Fig. 2. Bilinear idealization of the normal stress in a crack as a function of the normal crack strain.

the shear stress carrying capacity of the crack faces due to aggregate interlock is not important in a direct tensile test where we primarily expect normal crack strains. To avoid possible energy consumption in spurious crack shear displacements (Rots *et al.*, 1985) the term D^{cr}_{22} has therefore also been set equal to zero. Hence, $\mathbf{D}^{cr}$ reduces to

$$\mathbf{D}^{cr} = \begin{bmatrix} D^{\mathrm{I}} & 0 \\ 0 & 0 \end{bmatrix}. \tag{7}$$

The tensile-softening modulus D^{I} sets the relation between the normal stress rate in the crack and the normal crack strain rate. It can be related to three basic tensile-softening parameters, namely the uniaxial tensile strength f_{ct}, the mode-I fracture energy G_f (defined as the amount of energy required to create one unit of area of a pure mode-I crack) and the shape of the tensile-softening diagram. Especially the shape of the softening diagram is important (Hillerborg *et al.*, 1976; Rots, 1986) and according to various experiments (Cornelissen *et al.*, 1986; Gopalaratnam and Shah, 1985; Hordijk *et al.*, 1987; Labuz *et al.*, 1985) it seems reasonable to assume a tensile-softening function with a steep drop after the peak stress followed by a long tail. Three different softening curves, namely a linear, a bilinear and a nonlinear diagram have been adopted in this paper to study the effect of the shape of the diagram. If no further information is given, it is implied that the bilinear diagram of Fig. 2 is used. It is further noted that unloading and reloading have been modelled using a secant approach, as also indicated in Fig. 2.

The fracture energy G_f is assumed to be a fixed material constant, which seems to be justified because the energy required to fracture mode-I specimens is fairly proportional to the surface area generated. In a smeared crack approach, fracture is spread over a crack band width h, which is related to the particular finite element configuration. In the case of four-noded elements with a single integration point, as has been used in the elements through which the crack propagated, the element width must be inserted for the crack band width h.

4. COMPUTATIONAL PROCEDURES

In the experiment the load was applied at point G and was servo-controlled by a feedback signal from two LVDTs mounted at the sides of the specimen (Fig. 1a). In the numerical simulation, the analysis has been carried out using "indirect displacement control". This procedure (de Borst, 1987) is a modification of the arc length method proposed by Riks (1979). It considers the load increment as a variable rather than as a fixed quantity and the value of the load increment is determined by constraining some dominant displacement increment. In the present study, the crack opening displacement increment of the active notch served as the control parameter. As we will notice in the next section, crack propagation in direct tension tests usually proceeds from one notch to the
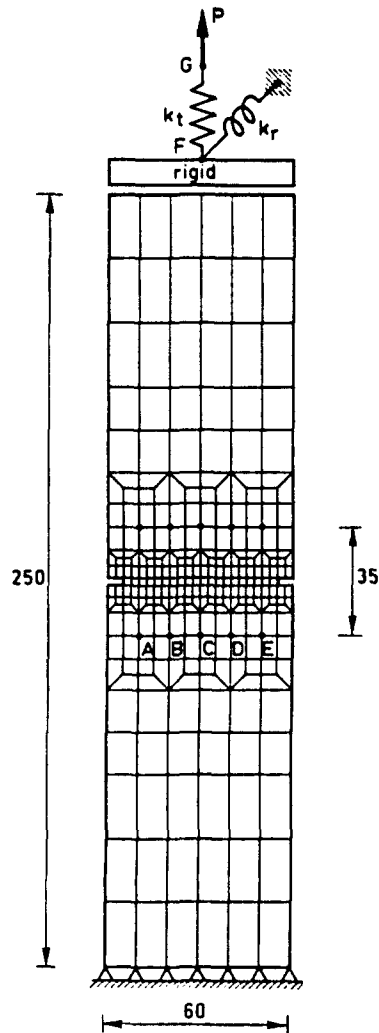
Fig. 3. Finite element mesh for analysis of the direct tension test.

opposite notch, whereby only one notch is active at a time. For most of the analyses reported in this paper it appeared to be absolutely necessary to apply the constraint equation *only* to the active notch in order to properly overcome the limit point. In the vicinity of the limit point it furthermore appeared necessary to use a full Newton–Raphson iterative procedure with the tangent stiffness matrix being updated at the beginning of each iteration.

5. COMPUTATIONAL RESULTS

In this section the double-notched tensile specimen of Fig. 1a is analysed using the crack model previously described. Figure 3 shows the finite element idealization, which consists of four-noded bilinear elements with four-point Gauss quadrature. An exception was made for the centre row of elements between the notches, which were integrated using a reduced 2 * 1 point integration scheme, see also Rots (1986).

The lower boundary of the specimen was assumed to be fixed, while in the reference calculation a translational spring and a rotational spring have been added at the upper boundary in order to simulate the effect of the testing machine. The spring stiffnesses were specified as $k_t = 148,000$ N/mm and $k_r = 10^9$ Nmm/rad. Constraint equations were added to the global system of equations so as to ensure that the top of the specimen be kept straight. In this manner, the upper boundary could undergo a translation and a rotation but no distortion.

The elastic concrete properties have been assumed to be: Young's modulus $E = 18,000$

N/mm^2 and Poisson's ratio $v = 0.2$, which corresponds to a lightweight concrete specimen. The softening parameters have been taken as: tensile strength $f_{ct} = 3.4 \, N/mm^2$ and fracture energy $G_f = 59.3 \, J/m^2$. The fracture has been assumed to localize within the centre row of elements so that the crack band width was set equal to $h = 2.5$ mm. In some of the calculations one element in front of the right-hand notch of Fig. 3 was given a small material imperfection in the sense that the fracture energy G_f was reduced by 1 per cent. The importance of this imperfection will appear in the sequel to this paper.

We will first describe the analysis which will serve as a reference calculation. In this analysis the springs as specified above were included in the finite element model, the bilinear softening curve for the smeared-out cracks was used (Fig. 2) and an imperfection was inserted in front of the right-hand notch. The analysis progressed as shown in Figs 4a–4e, which represent key events in the fracture localization process. Upon incrementing the load the analysis started to predict symmetric deformations within the specimen, as shown in Fig. 4a which gives the incremental deformations at an average stress $\sigma = 2.837 \, N/mm^2$ (average stress and displacement as defined in Section 2). During the entire pre-peak regime of the load–displacement response the specimen appeared to be strained symmetrically, with both notches being active. A limit point was encountered at $\sigma = 2.856 \, N/mm^2$ and the tangent stiffness matrix ceased to be positive definite. Indeed, a negative eigenvalue was calculated for the tangent stiffness matrix. The incremental displacement field at peak load which has been plotted in Fig 4b shows a strongly non-homogeneous and non-symmetric deformation of the specimen. Obviously the right-hand notch with the small material imperfection suddenly becomes very active while the opposite side of the specimen unloads.

After locating the limit point, the load was decremented and a genuine equilibrium path could be obtained. Fracture localization propagates towards the opposite notch, as is shown in Fig. 4c which gives the incremental deformations at a residual average stress level $\sigma = 1.865 \, N/mm^2$. Upon a further decrease of the load, the left-hand notch became active again, while the right-hand notch tended to unload temporarily (Fig. 4d). Subsequently, the load had to be incremented again slightly to re-load the right-hand notch and to "stretch the specimen uniformly". After this operation all elements between the notches showed softening and the load could come down to zero under subsequent symmetric deformations (Fig. 4e).

The subsequent stages of incrementation and decrementation of the load can be recognized from Fig. 5, which gives the averaged stress–deformation curve (over the 35 mm gauge length). In Fig. 5 (and also in Fig. 6 which shows a close-up of Fig. 5 near the limit point) the non-symmetric solution is compared with the solution which was obtained by considering only a symmetric half of the specimen, thereby enforcing symmetric crack propagation. It appears that non-symmetric deformations reduce the limit load and, even more interestingly, have a significant impact on the post-peak part of the curve. While the symmetric solution describes a descending branch which reasonably resembles the bilinear input diagram (Fig. 2), the non-symmetric solution results in a steeper drop after the peak stress and in a significant "bump". The agreement with the experimental measurement of Fig. 1b is evident and proves that the "bump" is a direct consequence of the non-symmetric fracture mode which occurs in a strain-softening tensile test.

6. THE DIRECT TENSION TEST AS A BIFURCATION PHENOMENON

The material imperfection has been applied in the previous analysis to trigger non-symmetric crack propagation. Effectively, inserting a weak spot as has been done here transfers a bifurcation problem into a limit problem. Without the imperfection, the tension specimen will continue to deform symmetrically also in the softening regime of the load–displacement curve. Such an analysis has been carried out and resulted in the curve which is labelled as "symmetric" in Figs 5 and 6. Of course, this curve is identical to the curve that is obtained when only a symmetric half of the specimen is analysed. Yet, when analysing the full specimen, uniqueness of solution is lost before the peak stress is attained. For $\sigma = 2.866 \, N/mm^2$ a negative eigenvalue is extracted for the tangent stiffness matrix. The corresponding eigenmode is shown in Fig. 7a and clearly involves non-symmetric defor-
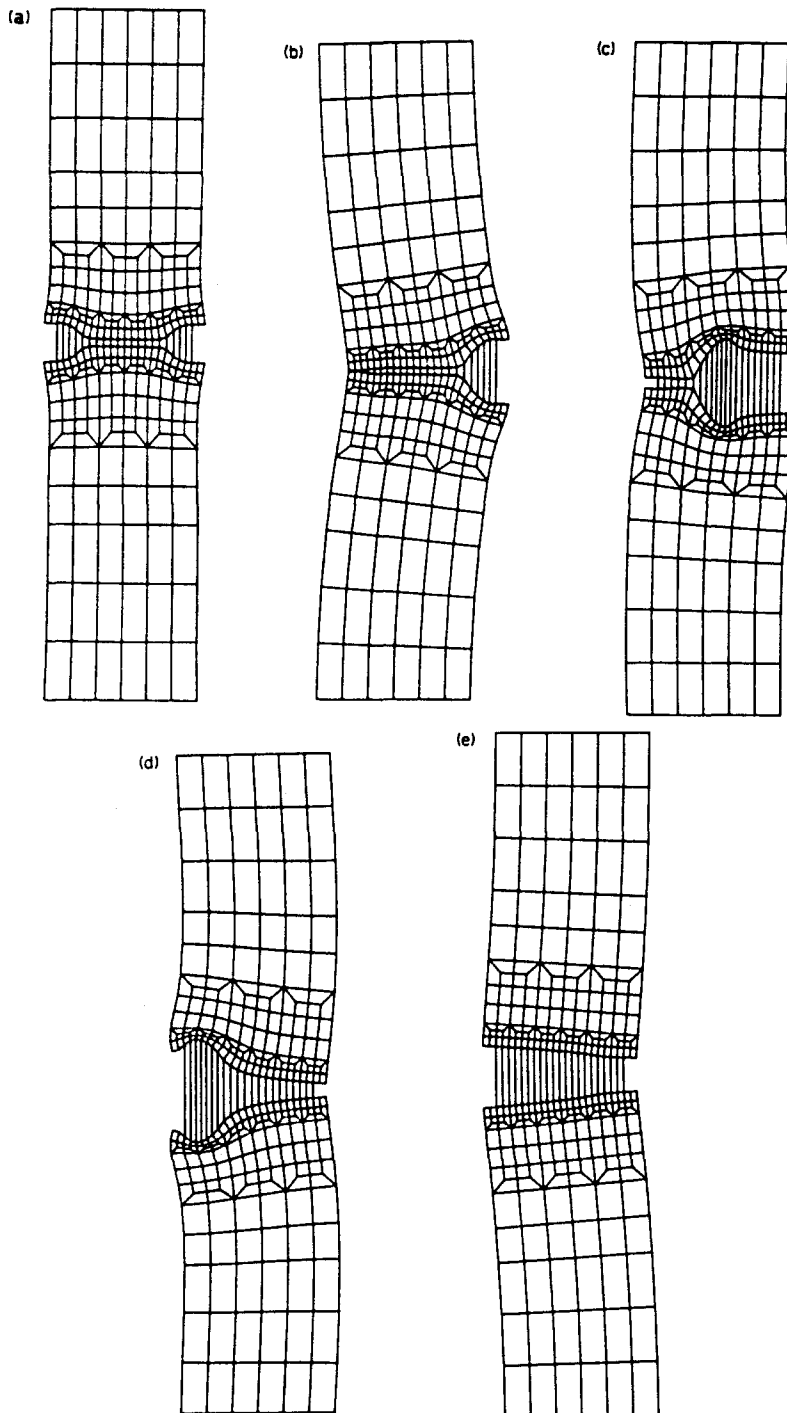
Fig. 4. Incremental displacements. (a) Prior to the peak load, $\sigma = 2.837$ N/mm^2. (b) At the peak load, $\sigma = 2.856$ N/mm^2. (c) Beyond the peak load, $\sigma = 1.865$ N/mm^2. (d) Beyond the peak load, $\sigma = 1.101$ N/mm^2. (e) Beyond the peak load, $\sigma = 1.026$ N/mm^2.

mations. This so-called bifurcation point marks the beginning of an alternative equilibrium path that involves non-symmetric deformations. Continuation on this path can be enforced by adding a part of the eigenvector to the incremental displacement vector (de Borst, 1987). In the present calculation this possibility has not been pursued, and further incrementation of the load resulted in continued symmetric deformations. A second negative eigenvalue of the tangent stiffness matrix is encountered at $\sigma = 2.887$ N/mm^2. The second eigenmode is plotted in Fig. 7b. After the emergence of the second negative eigenvalue, further incrementation of the load appeared to be not possible, and an equilibrium path could only be
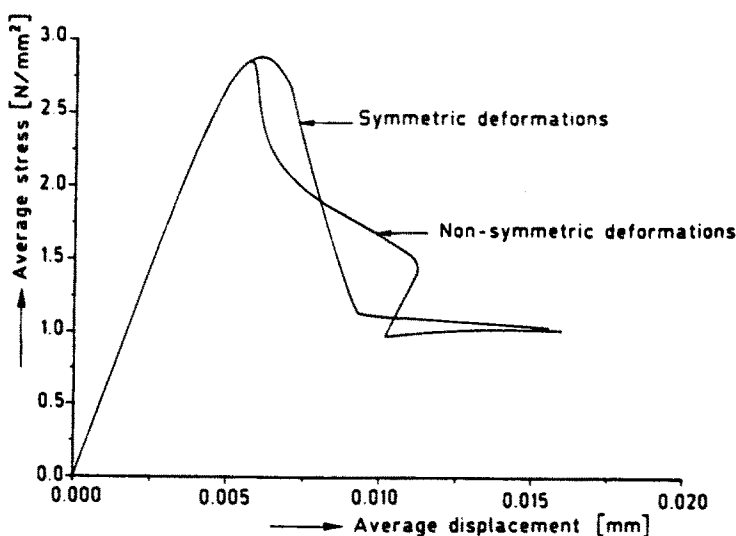
Fig. 5. Average stress as a function of the average deformations over a gauge length of 35 mm.
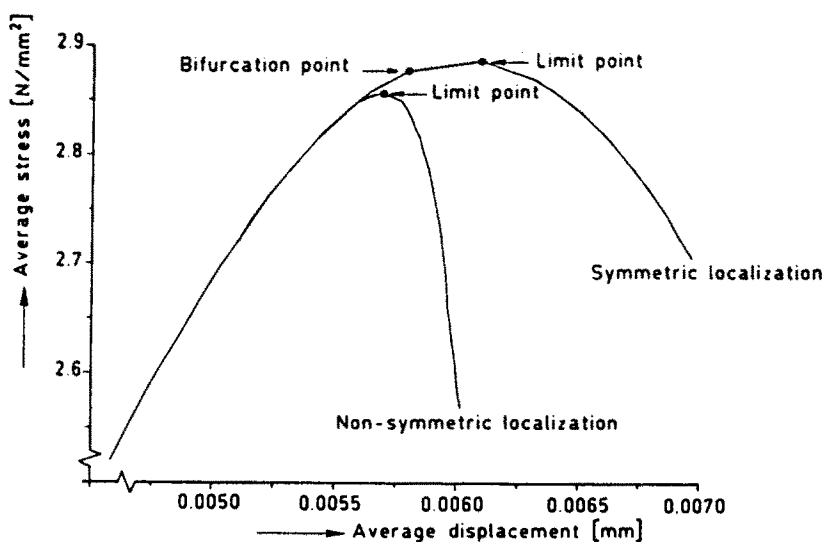

Fig. 6. Enlarged graph of the average stress as a function of the average deformations over a gauge length of 35 mm

obtained by decrementing the load. Consequently, the second negative eigenvalue is related to a limit point.

In the real world, imperfections always exist and it is unimaginable that crack propagation will ever be symmetric in the direct tension test. An exception are perhaps very short specimens, where the role of the boundary conditions is so dominant that they prevent asymmetric crack propagation.

The observation that the asymmetric failure mode results in the steepest post-peak load–deformation path not only pertains to crack propagation in concrete or rock, neither is it exclusive to this type of test. It is valid whenever a material model in which ellipticity is lost at a generic stage in the loading process is used in a calculation of a structure in which some kind of symmetry, antisymmetry or axisymmetry occurs. Examples involving soil plasticity have been published by de Borst (1989).

7. THE EFFECT OF THE SOFTENING CURVE

In the past few years there has been much debate on the validity of the applicability of G_f concepts to fracture of concrete and rock, e.g. van Mier (1986). With regard to this
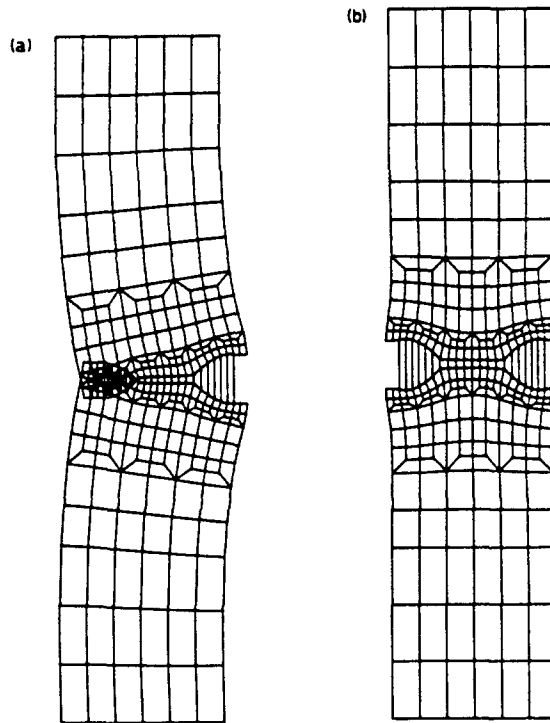
Fig. 7. (a) Eigenmode that corresponds to the first negative eigenvalue (bifurcation point).
(b) Eigenmode that corresponds to the second negative eigenvalue (limit behaviour).

issue, we first want to express our opinion that continuum descriptions *can* be used to simulate failure processes in solids that show a deterioration of the load-carrying capacity with increasing deformation. Upon transformation of the load-displacement curve into a *local* stress-strain diagram at integration point level such a deterioration manifests itself as a descending branch and is usually named *strain* softening. Although we have the opinion that continuum descriptions are still applicable to such solids, we support the widespread view that *non-local*, e.g. Bažant (1986), Pijaudier-Cabot and Bažant (1987), Schreyer and Chen (1986), or *polar*, e.g. Mühlhaus and Vardoulakis (1987), models must be used so as to regularize the governing continuum equations. Nevertheless, such an approach may well call for an extremely fine element division, since the element width must be smaller than the characteristic length in order to properly capture the localization process. For simulation of experiments on small specimens such an approach is probably feasible with the computers that are currently available. Use of such a model clearly becomes unwieldy for large-scale engineering applications such as storage vessels or dams. Indeed, for very large concrete structures or rock masses a linear-elastic fracture mechanics approach is often used successfully, e.g. Bažant (1986), Saouma *et al.* (1982). The used local softening model with a G_f concept has merit for analysing structures of an intermediate size, which are too small for application of linear-elastic fracture mechanics, but too big for a delicate analysis using non-local or polar continua. It is thus believed that even with the advent of such improved, non-classical continuum descriptions, local softening models will remain useful.

However, if we want the G_f concept to be successful we must pay proper attention to the determination of its parameters. Especially the shape of the softening diagram is important as has been emphasized before by Rots (1986) for problems involving indirect tension. Here, we will show that a proper shape of the softening diagram is crucial for a successful simulation of the fracture process in direct tension.

It has been mentioned in the preceding discussion that three different shapes of the softening diagram have been used in this study, namely a linear diagram, a bilinear diagram (Fig. 2) and the nonlinear diagram proposed by Cornelissen *et al.* (1986) and Hordijk *et al.* (1987). The parameters of the bilinear diagram have been selected such that this diagram has the steepest slope for small crack strains. The same values for the tensile strength f_{ct}
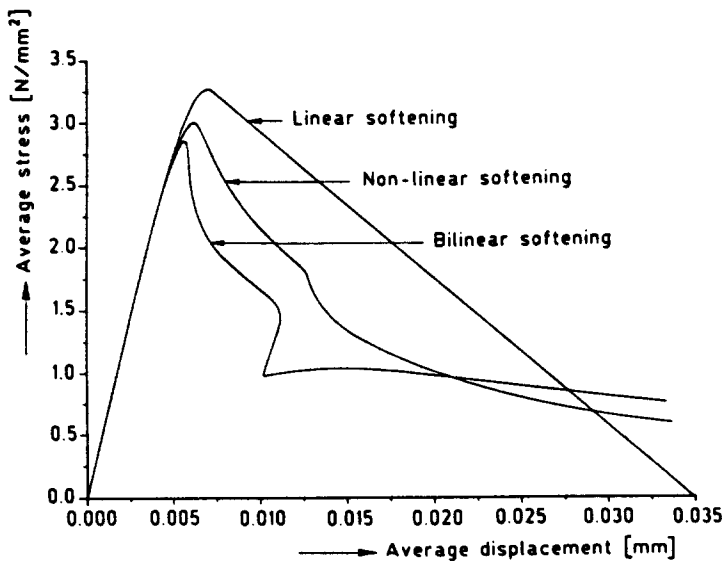
Fig. 8. Average stress as a function of the average deformations over a gauge length of 35 mm for different softening curves.

and for the fracture energy G_f were adopted in the three analyses (respectively 3.4 N/mm^2 and 59.3 J/m^2). The boundary conditions were also taken equal in all the analyses (with a translational and a rotational spring at the upper boundary) and a weak element was placed in front of the right-hand notch.

The results are represented in Fig. 8. A first observation, also made by Rots (1986) for indirect tension, is that the peak load is influenced. For the same f_{ct} and G_f a higher load-carrying capacity is found for the linear softening curve than for the nonlinear and the bilinear curves. The bilinear curve, with the steepest slope immediately after cracking, produces the lowest limit load. More interesting, though, is the structural post-peak behaviour. Then, the nonlinear and the bilinear curves result in asymmetric crack propagation and an accompanying "bump" in the load-displacement curve, the "bump" again being more pronounced for the bilinear diagram. When a linear softening diagram is used, however, the specimen continues to deform symmetrically in the softening regime. A "bump" in the load-displacement curve is not found and the calculated load-displacement curve is almost identical to the stress-strain diagram that served as input for the analysis. This result is in clear contradiction with the experimental data by Cornelissen *et al.* (1986) and Hordijk *et al.* (1987). Evidently, use of a linear softening diagram yields incorrect results. On the other hand, the bilinear diagram probably exaggerates the phenomenon. The nonlinear curve proposed by Cornelissen *et al.* (1986) and Hordijk *et al.* (1987) seems to produce the results that most closely match experimental data. Yet, some caution must be exercised in drawing quantitative conclusions, since the analyses have been carried out under the assumption of plane stress, while three-dimensional effects definitely play a role in this experiment with the crack front not only propagating from right to left, but also from the front to the back of the specimen (or vice versa). Basically, crack propagation from the front to the back of the specimen introduces a further source of structural behaviour in the softening curve for plane-stress analysis.

8. THE EFFECT OF THE BOUNDARY CONDITIONS

Apart from subtleties in the adopted constitutive model the response of a structure composed of strain-softening material may heavily depend on the boundary conditions. For example, tilting of the end platens may drastically affect the outcome of the experiment. We will show that the effect of the boundary conditions in this experiment is negligible.

To this end, the analyses with the bilinear and with the linear softening curve have been carried out also for the case that the upper platen is free to rotate and for the case that the
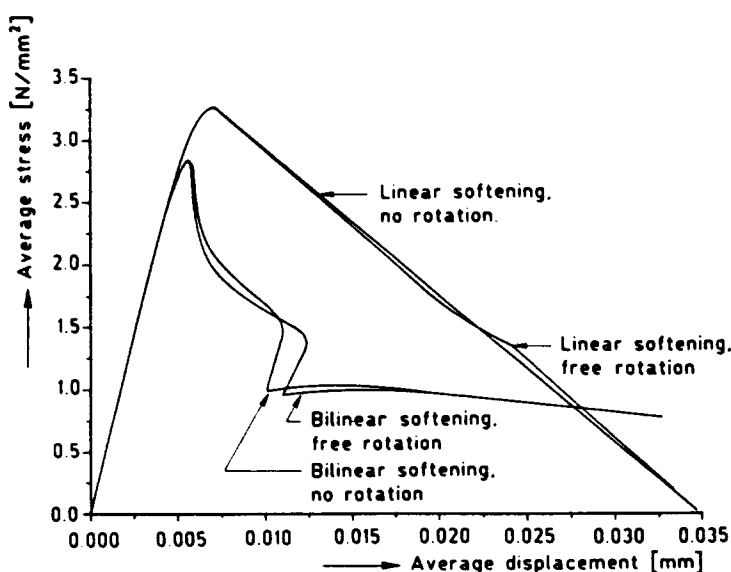
Fig. 9. Average stress as a function of the average deformations over a gauge length of 35 mm for different boundary conditions.

rotation of the upper platen is completely prohibited. Distortion of the upper boundary was not allowed in either of both cases. The results are shown in Fig. 9. It appears that the boundary conditions hardly have any impact on the load-displacement curve and on the fracture process. For the bilinear softening curve the free rotating end platen merely yields a slightly more pronounced snap-back behaviour compared to the fixed upper platen, but the characteristics of the failure process, namely the typical "bump" and the fact that both notches become active one after the other, are present in both analyses. These findings contradict conclusions reached by van Mier (1986), who argued that for a free rotating end platen the "bump" cannot occur.

For the linear softening curve we observe that the free boundary allows asymmetric crack propagation during a small part of the deformation process. This temporary asymmetry is accompanied by a minor deviation from linearity in the load-displacement curve. The fixed boundary completely suppresses any asymmetry in crack propagation and the resulting load-displacement curve is linear.

In conclusion there is some influence of the boundary conditions, but the effect is of minor importance in direct tensile tests on specimens of this length. When considering shorter specimens, or compression tests as for instance have been carried out by van Mier (1986), the influence of the boundary conditions is more significant. In this respect, it is worth mentioning that a calculation on a specimen with a length of 125 mm yielded symmetric crack propagation also for the nonlinear softening curve. This calculation supports experimental observations by Hordijk et al. (1987) who concluded that asymmetric crack propagation and a "bump" are not observed for very short specimens.

9. SNAP-BACK BEHAVIOUR

Considering the load-displacement path in Fig. 5 that corresponds to the non-symmetric deformations, we observe that when the left-hand notch becomes active again, not only the load but also the displacement decreases. This so-called "snap-back" behaviour can be illustrated even better if we plot the stress-deformation over a gauge length which is longer than 35 mm. To this end, the averaged stress has been plotted against the total elongation of the specimen in Fig. 10, so that the reference length is now equal to 250 mm.

Figure 10 exhibits a pronounced snap-back phenomenon after peak. The importance of this phenomenon was recognised before by e.g. de Borst (1986), Carpinteri et al. (1986) and Crisfield (1986), and entirely explains why direct displacement control, in which the displacements of the top of the sample are prescribed directly rather than applying the load
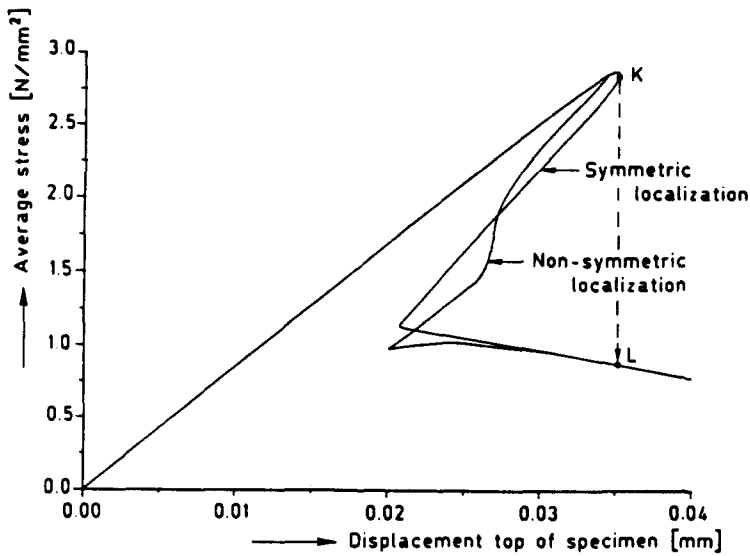
Fig. 10. Average stress as a function of the end displacement of the specimen.

directly and adjusting the load level such that the elongation over the gauge length in a loading step is equal to a prescribed value, cannot produce a truly converged solution beyond peak load. Similar conclusions can be reached for a number of other experiments on plain concrete which are available in the literature (de Borst, 1987; Rots and de Borst, 1987; Rots, 1988). If the present analysis had been carried out under direct displacement control at the top of the specimen, the quasi-static solution would have had to jump from point K to point L in Fig. 10, leaving the interesting part of the load–displacement curve with the "bump" undetected. Clearly, indirect displacement control with a proper control parameter is essential for analysing the post-peak response (de Borst, 1987). In Section 4 it has been argued that keeping track of the active notch is sometimes the only feasible control mechanism. This statement is supported by Fig. 5 which shows that the increment of the average deformation over a gauge length of 35 mm becomes negative for a particular part of the post-peak regime. Consequently, the average crack opening displacement of both notches cannot be employed as an effective control parameter during the entire deformation process. Neither can the crack opening displacement of any of the notches be used during the entire deformation process, since they both become passive at a certain stage of the deformation process and then exhibit negative increments of the notch opening (Fig. 11). Guiding the solution by controlling the crack opening of the active notch is the only solution.

In addition, the snap-back phenomenon explains the difficulties which have been encountered frequently in closed-loop tensile testing. The importance of a proper feedback signal over a short gauge length which encompasses the fracture zone has been emphasized by e.g. Gopalaratnam and Shah (1985) and Labuz et al. (1985) and is supported by the present numerical investigation. If this requirement is not met, an unstable response may be generated as the signal monitors unloading outside the fracture zone rather than softening within the fracture zone. Depending on the precise elastic-softening properties of the material even a gauge length of 35 mm may not be small enough to circumvent snapback phenomena.

10. CONCLUSIONS

Novel computational techniques and a continuum based elastic-softening model have been applied to simulate the strain-softening behaviour of concrete in a direct (uniaxial) tension test. It has been shown that the structural behaviour after the peak load involves strongly non-symmetric deformations, which entirely parallels experimental observations (Cornelissen et al., 1986; Hordijk et al., 1987; Labuz et al., 1985). It is therefore concluded
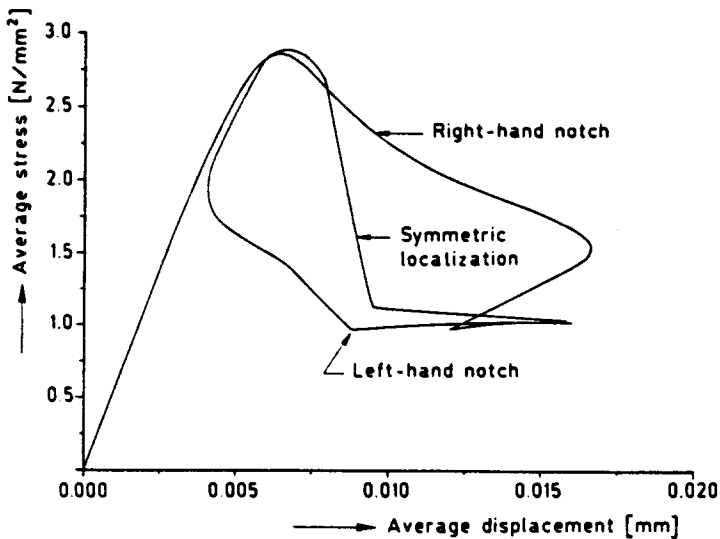
Fig. 11. Average stress as a function of the deformations of the right-hand and the left-hand notch over a gauge length of 35 mm.

that a "direct" tensile test on a heterogeneous material is generally not as direct as the name suggests.

A consequence of non-symmetric deformations is that the descending branch measured in direct tensile tests cannot be considered as a pure "material" property. Instead, such a curve is the outcome of a combination of material behaviour, described by the elastic-softening parameters for the equivalent, homogenized continuum, and structural behaviour due to non-homogeneous and often strongly localized deformations for that specific structure and set of boundary conditions. The importance of structural effects has been recognized before, e.g. van Mier (1986), Read and Hegemier (1984), and the question has arisen whether it makes sense to derive softening functions from such tests. In other words, may we implement softening functions measured in a particular test in a general purpose finite element code and then use that code to predict the response of an arbitrary structure that is composed of a strain-softening material?

The above results indicate that we may not unrestrictedly do so, since this would imply extrapolation of "bumps", which have been shown to be merely the result of non-symmetric deformations, and other structural effects to different circumstances. However, by properly combining experimental results and numerical simulations it may be possible to arrive at a set of elastic-softening parameters which objectively triggers fracture under different boundary conditions and different geometries. According to the present investigation, the introduction of a true "unnotched tensile strength" which exceeds the "notched tensile strength", as well as the inclusion of a nonlinear softening diagram with a steep drop just after peak stress seem essential ingredients. Further research is required in order that quantitative conclusions be drawn on this issue.

Snap-back behaviour, which is known to be possible in strain-softening solids (de Borst, 1986; Carpinteri et al., 1986; Crisfield, 1986), has been demonstrated to dominate the response of concrete in a direct tensile test. This phenomenon requires proper feedback signals, both in experiments and in computations.

REFERENCES

Bažant, Z. P. and Oh, B. H. (1983). Crack band theory for fracture of concrete. RILEM Mater. Construct., Paris 16, 155–177.

Bažant. Z. P. (1986). Mechanics of distributed cracking. *Appl. Mech. Rev.* **39**, 675–705.

de Borst, R. and Nauta, P. (1985). Non-orthogonal cracks in a smeared finite element model. *Engng Comput.* **2**, 35–46.

de Borst, R. (1986). Non-linear analysis of frictional materials. Dissertation, Delft University of Technology, Delft.

de Borst, R. (1987). Computation of post-bifurcation and post-failure behaviour of strain-softening solids. *Comput. Struct.* **25**, 211–224.

de Borst, R. (1989). Numerical methods for bifurcation analysis in geomechanics. *Ing. Arch.* **59**, 160–174.

Budnik, J. (1985). Bruch- und Verformungsberhalten harzmodifizierter und faserverstärkter Betone bei einachsiger Zugbeanspruchung. Dissertation, Ruhr-Universität Bochum, Bochum.

Carpinteri, A., Di Tomasso, A. and Fanelli, M. (1986). Influence of material parameters and geometry on cohesive crack propagation. In *Fracture Toughness and Fracture Energy of Concrete* (Edited by F. H. Wittmann), pp. 117–135. Elsevier, Amsterdam.

Cornelissen, H. A. W., Hordijk, D. A. and Reinhardt, H. W. (1986). Experimental determination of crack softening characteristic of normal weight and lightweight concrete. *HERON* 31(2), 45–56.

Crisfield, M. A. (1986). Snap-through and snap-back response in concrete structures and the dangers of under-integration. *Int. J. Numer. Meth. Engng* **22**, 751–768.

Gopalaratnam, V. S. and Shah, S. P. (1985). Softening response of plain concrete in direct tension. *J. Am. Concr. Inst.* **82**, 310–323.

Hillerborg, A., Modeer M. and Petersson, P. E. (1976). Analysis of crack formation and crack growth in concrete by means of fracture mechanics and finite elements. *Cem. Conc. Res.* **6**, 773–782.

Hordijk, D. A., Reinhardt, H. W. and Cornelissen, H. A.W. (1987). Fracture mechanics parameters of concrete from uniaxial tests as influenced by specimen length. *Proc. SEM-RILEM Int. Conf. on Fracture of Concrete and Rock* (Edited by S. P. Shah and S. E. Swartz), pp. 138–149. Soc. Exp. Mechanics, Bethel.

Labuz, J. F., Shah, S. P. and Dowding, C. H. (1985). Experimental analysis of crack propagation in granite. *Int. J. Rock Mech. Min. Sci. Geomech. Abstr.* **22**, 85–98.

van Mier, J. G. M. (1986). Fracture of concrete under complex stress. *HERON* 31(3).

Mühlhaus, H. B. and Vardoulakis, I. (1987). The thickness of shear bands in granular materials. *Geotechnique* **37**, 271–283.

Pijaudier-Cabot, G. and Bažant, Z. P. (1987). Nonlocal damage theory. *ASCE J. Engng Mech.* **113**, 1512–1533.

Read, H. E. and Hegemier, G. A. (1984). Strain-softening of rock, soil and concrete—A review article. *Mech. Mater.* **3**, 271–294.

Riks, E. (1979). An incremental approach to the solution of snapping and buckling problems. *Int. J. Solids Structures* **15**, 529–551.

Rots, J. G., Nauta, P., Kusters G. M. A. and Blaauwendraad, J. (1985). Smeared crack approach and fracture localisation in concrete. *HERON* 30(1).

Rots, J. G. (1986). Strain-softening analysis of concrete fracture specimens. *Fracture Toughness and Fracture Energy of Concrete* (Edited by F. H. Wittmann), pp. 137–148. Elsevier, Amsterdam.

Rots, J. G. and de Borst, R. (1987). Analysis of mixed-mode fracture in concrete. *ASCE J. Engng Mech.* **113**, 1739–1758.

Rots, J. G. (1988). Computational modeling of concrete fracture. Dissertation, Delft University of Technology, Delft.

Saouma, V., Ingraffea, A. R. and Catalano, D. (1982). Fracture toughness of concrete: K_{Ic} revisited. *ASCE J. Engng Mech. Div.* **108**, 1152–1166.

Schreyer, H. L. and Chen, Z. (1986). One-dimensional softening with localization. *J. Appl. Mech.* **53**, 791–979.

Walraven, J. C. and Reinhardt, H. W. (1981). Theory and experiments on the mechanical behaviour of cracks in plain and reinforced concrete subject to shear. *HERON* 26(1A).

Willam, K., Hurlbut, B. and Sture, S. (1986). Experimental and constitutive aspects of concrete failure. *Finite Element Analysis of Reinforced Concrete Structures.* (Edited by C. Meyer and H. Okamura), pp. 226–254. ASCE, New York.